ADVANCED MATERIALS INTERFACES
www.advmatinterfaces.de

Self-Powered Multifunctional Human–Machine Interfaces for Respiratory Monitoring and Smart System Control

*Yaokun Pang, Shoue Chen, Yunteng Cao, Zhida Huang, Xianchen Xu, Yuhui Fang, and Changyong (Chase) Cao**

Innovative human–machine interfaces (HMIs) have attracted increasing attention in the field of system control and assistive devices for disabled people. Conventional HMIs that are designed based on the interaction of physical movements or language communication are not effective or appliable to severely disabled users. Here, a breath-driven triboelectric sensor is reported consisting of a soft fixator and two circular-shaped triboelectric nanogenerators (TENGs) for self-powered respiratory monitoring and smart system control. The sensor device is capable of effectively detecting the breath variation and generates responsive electrical signals based on different breath patterns without affecting the normal respiration. A breathing-driven HMI system is demonstrated for severely disabled people to control electrical household appliances and shows an intelligent respiration monitoring system for emergence alarm. The new system provides the advantages of high sensitivity, good stability, low cost, and ease of use. This work will not only expand the development of the TENGs in self-powered sensors, but also opens a new avenue to develop assistive devices for disabled people through innovation of advanced HMIs.

1. Introduction

There is a large population, about one billion people (up to 15% of the total population in the world) with some form of disability according to data from the World Health Organization (WHO).[1,2] Those disabled people suffer much in their daily life and need intensive assistance and care from family members or professional caregivers, causing poor life quality and substantial burdens on family and society. Over the past few decades, many assistive technologies have been proposed to improve the living quality and wellness of disabled people. Among them, the human–machine interface (HMI) that can communicate and interact between human and the digitalized world has attracted increasing attention.[3,4] The conventional HMI devices, such as smart watches, smart bracelets, glasses, and smart clothing, mainly designed based on physical interactions or language communication,[5–7] are suitable for healthy people or disabled people with good control and moving ability.[8] However, for people with severe damage to their body functionality, such as quadriplegia, amyotrophic lateral sclerosis, or locked-in syndrome, the common HMI will not meet the requirements because the users cannot express their minds clearly and easily through muscular motion or language communication.

Recently, some advanced HMIs were developed for those severely disabled people, including brain-computer interface (BCI), electromyography (EMG) switch, eye gaze tracker, and sniff controller.[9–14] The BCI is based on electroencephalogram (EEG) signals and considered as the most promising technology to assist disabled people due to its low set-up costs, ease-of-use, and noninvasive nature. It has been used to control robots with limited success. The major challenges to its wide applications include: the low signal-to-noise ratio of the scalp-recorded EEG signals (in microvolts), strong interference, slow response time, and higher requirements for the classification algorithm.[9,10] EMG is another main tool used to capture users' intentions and emotions.[11,12] However, it usually uses needles to puncture the skin or attaches the electrodes onto the body surface, which are uncomfortable, difficult to setup, and not aesthetically appealing. Researchers also invented eye gaze trackers to analyze and measure eye positions and eye movement to perform communication and control with the external

Y. Pang, S. Chen, Z. Huang, X. Xu, C. (Chase) Cao
Laboratory for Soft Machines & Electronics
Department of Mechanical and Aerospace Engineering
Case Western Reserve University
Cleveland, OH 44106, USA
E-mail: ccao@case.edu

Y. Pang
State Key Laboratory of Bio-Fibers and Eco-Textiles
Collaborative Innovation Center of Marine Biobased Fiber and Ecological Textile Technology
Institute of Marine Biobased Materials
School of Materials Science and Engineering
Qingdao University
Qingdao 266071, China

Y. Cao
Department of Civil and Environmental Engineering
Massachusetts Institute of Technology
Cambridge, MA 02139, USA

Y. Fang
4D Maker LLC
Okemos, MI 48864, USA

The ORCID identification number(s) for the author(s) of this article can be found under https://doi.org/10.1002/admi.202201202.

DOI: 10.1002/admi.202201202

world.[13,14] Such designs need to deploy electrodes around the eyes or a camera mounted in front of the face, which generates uncomfortable feelings and affect visual sights.[15,16]

Breathing or respiration is one of the basic living features of humans. Therefore, even if the users are severely hurt and lose their hearing, language, and/or motion ability, they will still have the ability of respiration. Typically, humans can rapidly regulate their breath intensity and rhythm, and change airflow rate within 160 ms in response to different odorants.[17] Therefore, breath-based HMI can be an ideal tool for severely disabled people. For example, Plotkin et al. developed a breathing controller system that measured nasal pressure. They converted it into electrical signals, realizing the functions of controlling an electric wheelchair and writing text.[18] However, a nasal cannula was used to carry nasal pressure to the sensor powered by a battery, which makes patients feel uncomfortable and may affect normal breathing.

Triboelectric nanogenerator (TENG), based on the coupling effect of triboelectrification and electrostatic induction, has been demonstrated as a powerful technology for converting pervasive mechanical energy into electrical energy.[19–24] It has been widely used for energy harvesting and self-powered sensors to detect mechanical motions and deformations due to its simple mechanism, low cost, high sensitivity, and remarkable adaptability.[25–28] Mao et al. proposed air-flow-driven TENGs for developing breathing sensors integrated with a mask.[29,30] However, they are heavy, bulky, and uncomfortable to wear. Moreover, the working stability of the breath sensors was poor due to the influence of the exhaled moisture. Therefore, it is highly desirable to design a portable, sensitive, stable, comfortable, and self-powered HMI for severely disabled people for an easy life with high living quality.

In this paper, we report a novel triboelectric sensor for respiratory monitoring and HMI system (**Figure 1**a). This sensor consists of a small soft fixator inserted into the nostrils and two circular-shaped TENGs based on single-electrode mode. The effects of critical factors, including the distance between the nose and the device, the thickness of the Ecoflex film, and the thickness and diameter of the circular spacer, on the sensing performance of the triboelectric sensor are studied in detail. The proposed device can effectively detect the breath variation and generate responsive electrical signals based on different breath patterns without affecting the normal respiration. Furthermore, by integrating it with a simple signal processing circuit, we demonstrate a smart breathing-driven HMI system for severely disabled people to control electrical household appliances and develop an intelligent respiration monitoring system for respiratory interruption alarm. This work provides an innovative strategy for respiration monitoring and paves the way for developing the next-generation HMI system for severely disabled people.

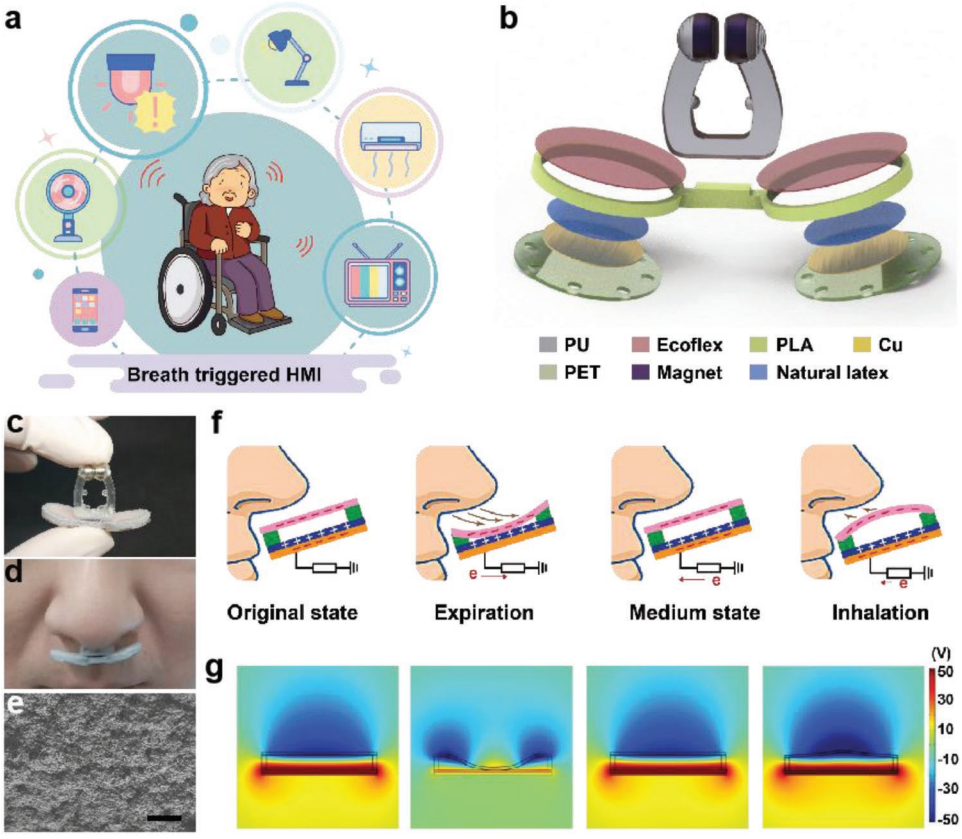

Figure 1. Structural design and working mechanism of the breathing-driven triboelectric sensor. a) Schematic diagram of the designed TENG-based HMI system. b) Schematic illustration of structural components of the triboelectric sensor. c,d) Photographs of the triboelectric sensor prototype. e) SEM image of the Ecoflex film with surface microstructures. Scale bar, 50 µm. f) Schematic illustration of the working principle of the triboelectric sensor. g) The electrical potential distribution in the two triboelectric layers of the sensor simulated by FEA.

2. Results and Discussion

2.1. Rational Design and Working Principle of the HMI

As shown in Figure 1b,c, the breathing-driven triboelectric sensor consists of two main components: a small soft fixator inserted into the nostrils and two circular-shaped TENGs under the nostrils. Traditional breathing sensors are usually integrated into a face mask that covers the nose tightly to detect the breathing airflow, which is not convenient and cannot be used for patients with asthma. Unlike previous studies, our device can be worn on the noses by a novel fixator (Figure 1d), consisting of a polyurethane (PU) holder and two small magnets. The small and soft PU holder can be easily inserted into the front of the nasal cavity without affecting the user's regular respiratory. Its size and shape can be personalized according to the preference and features of the wearers. On the top of the holder, two small coin magnets embedded in the PU holder are used to fix the fixator in the nasal cavity. Additionally, this fixator is lightweight, small, convenient, and independent on straps or tapes.

Figure 1b illustrates the schematic for the multi-layered structures of the TENG sensor based on a single-electrode mode. A thin circular-shaped polyethylene terephthalate (PET) sheet of 0.5 mm thick was used as the substrate. Eight hoes with a diameter of 1.4 mm were punched along the edge of the PET substrate to serve as airflow channels. A thin layer of copper film (75 μm thick) was bonded on the top surface of the PET substrate as the electrode. Then, a thin natural latex layer was laminated onto the electrode as one electrification layer. A 3D printed circular spacer made of polylactic acid (PLA) was used as the framework for the triboelectric sensor to hold the multiple layers. Its thickness and diameter will affect the sensing performance and can be optimized based on dynamic analysis. To enhance the sensor's sensitivity under small airflow pressures, an ultrathin Ecoflex film was utilized as the top electrification layer, which has the merits of high elasticity, high tensile strength, and strong electron affinity. In addition, surface microstructures were patterned on the surface of the Ecoflex film by using a sandpaper template, as shown in Figure 1e. The prototype of the fabricated triboelectric sensor is only ≈1.48 g and could be even lighter by adjusting the component dimensions and materials (Figure S1, Supporting Information).

The working principle of the proposed triboelectric HMI sensor is the conjugation of contact triboelectrification and electrostatic induction. Figure 1f illustrates the electrical signal generation process in the triboelectric sensor when the user breaths. In brief, at the initial state, the same number of charges with opposite polarities are generated on the latex film and the Ecoflex film after several friction cycles between the two triboelectric layers. When the user breaths, the exhaled airflow will drive the Ecoflex film to deflect and approach to the natural latex film. The potential difference between two surfaces will gradually decrease in this process, leading to an instantaneous electron flow from the Cu electrode to the ground. Therefore, a pulse output voltage is generated to the external load. When the Ecoflex film contacts the natural latex film with a large contact area, all the induced electrons are driven to the ground. Once the expiration process is complete, the Ecoflex triboelectric film will restore to its original state because of its excellent elasticity, leading to an opposite current flow in the external circuit. During the inhalation process, the Ecoflex film will vibrate slightly due to the weak suction, and a small number of electrons will flow between the Cu electrode and the ground, inducing a weak voltage signal. The electric potential distributions at the deformed states are calculated based on the finite element analysis (FEA), as shown in Figure 1g.

2.2. Sensing Performance of the Triboelectric Sensor

To assess the potential capability for respiration sensing, we have systematically investigated the electrical responses of the triboelectric sensor. As shown in Figure S2 (Supporting Information), an experimental setup was designed to characterize the sensor's voltage signal quantitatively. A computer-controlled linear motor was utilized to regulate the duration and time intervals of the airflow pulse. A pressure meter was employed to mimic the human breathing airflow to control the applied air pressure. The output voltage of the TENG depends on the relative ability of the triboelectric materials to lose or gain electrons.[19] Ecoflex has been demonstrated as an excellent electrification material with a strong negative charge affinity.[31] Due to the excellent properties and robustness of the Ecoflex film, we selected it as the controlled top electrification layer while replacing the bottom electrification layer with five different kinds of materials: FEP, Cu, PET, Nylon, and Latex. The output voltages generated by the HMI sensors with different triboelectric materials are shown in **Figure 2**a. It can be seen that the TENG with a natural latex layer generated a higher output voltage. This is because the natural latex has a stronger ability to lose electrons than the other four materials. Figure 2b shows the voltage signals of the HMI sensor under different frequencies ranging from 0.25 to 2 Hz. It can be seen that the output voltage increases significantly with airflow frequency, indicating that a faster breathing rate can lead to a higher voltage signal.

We further studied the effect of the distance between the human nose and the device and the thickness of the Ecoflex film on the output performance of the HMI sensor. As indicated in Figure 2c, the peak-to-peak magnitudes of the output voltage generated by the sensor monotonically decrease from 0.72 to 0.3 V with the increased distance from 2 to 7 mm. This is mainly because the airflow pressure applied on the Ecoflex membrane decreases with the increased distance, resulting in a reduced contact area and thereby a smaller voltage. It is worth noting that if the sensor is positioned too close to the nose, it will affect the normal breathing, while if it is arranged too far from the nose, HMI sensor will have a reduced sensitivity. With the analysis, we determine an optimal distance is around 2 mm for such a configuration. Figure 2d presents the peak-to-peak values of the output voltage as a function of the Ecoflex film thickness. The insets in the figure are the cross-section views of the fabricated Ecoflex films. It can be found that the output voltage is negatively correlated with the thickness of the Ecoflex film. As we expected, the thinner Ecoflex film will generate a larger deflection under the same applied pressure, thereby a larger contact area between the two electrification layers, which is consistent with our simulation results (Figure S2a,

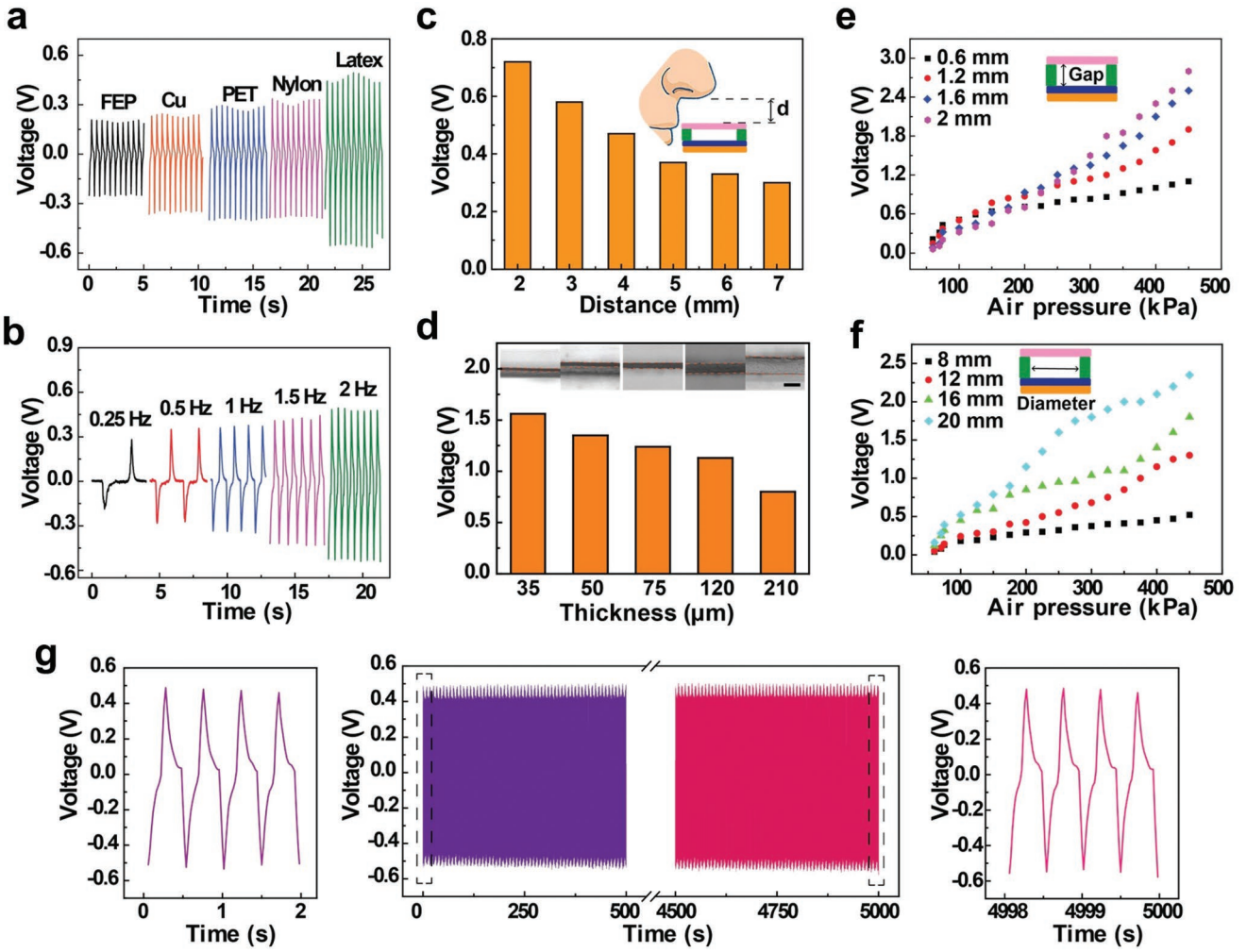

Figure 2. Sensing performance of the triboelectric sensor. a) Comparison of the output signals of the triboelectric sensors with different triboelectric substrates. b) Output signals of the triboelectric sensor under different actuation frequencies. c) Comparison of the output voltage by the triboelectric sensor with different distances between the nose and the sensor. d) Comparison of the output voltage of the sensor with different Ecoflex film thicknesses. The insets show the cross-section view of the fabricated Ecoflex film. Scale bar, 200 μm. e,f) Variation of the output signal with the gap distance and spacer size. g) The output voltage of the triboelectric sensor under repetitive testing of 10 000 cycles.

Supporting Information). Although a thinner Ecoflex film enables a more sensitive sensor with higher output voltage, a very thin film is difficult to be lifted off from the sandpaper template after surface microstructure patterning. Therefore, a thickness of 75 μm is chosen as the robust electrification layer in our prototypes used for the following experimental study.

In addition, we found that the sensitivity of the triboelectric sensor is significantly influenced by the gap distance and the spacer size, which affects the contact interactions between the two triboelectric films in perceiving the air pressure. Thus, to optimize the sensing performance, we fabricated four HMI sensors with circular spacers having different thicknesses (0.6, 1.2, 1.6, and 2 mm). Experimental data shows that under an air pressure ranging from 60 to 450 kPa, the output voltages of the triboelectric sensors increase with the applied air pressure (Figure 2e). When the air pressure is less than 100 kPa, the triboelectric sensor with a smaller gap has a larger output voltage and a higher sensitivity. This is mainly attributed to the smaller vibration amplitude of the Ecoflex film and thereby a good contact with the bottom electrification layer. On the contrary, in the high air pressure range (>100 kPa), the triboelectric sensors with larger gaps have higher output voltage, consistent with previous studies.[32,33] It should be noted that the applied air pressure here refers to the value shown in the gas outlet of a nitrogen tank (Figure S3, Supporting Information).

Figure 2f presents the effect of the circular spacer diameter (i.e., the size of the Ecoflex film) on the output voltage of the triboelectric sensor. A larger diameter results in a higher output voltage because of the larger contact area between the two triboelectric layers in the device (Figure S2b, Supporting Information). For long-term use, we have to study the reliability and stability of the device. As shown in Figure 2g, we performed more than 10 000 cycles of repeated loading–unloading of air pressure of 250 kPa at 2 Hz. There is no apparent degradation of the sensing signals observed, which demonstrates the excellent stability and durability of the HMI sensor. Based on the

insightful observations in this study, we will be able to optimize the design and configurations of the HMI sensor for personalized use with suitable sensing sensitivity and sensing range by adjusting the key factors.

2.3. Real-Time Respiration Monitoring via the Triboelectric Sensor

Respiration is one of the most essential physiological behaviors for maintaining human health conditions. Therefore, real-time respiration monitoring has become an indispensable practice for medical diagnosis and treatment. Our proposed design for the triboelectric sensor can be conveniently worn on the patient nose for respiration monitoring in a real-time manner. **Figure 3**a shows a real-time profile of the output voltage induced in one single cycle of respiration of a volunteer. As the volunteer is exhaling, the exhaled airflow leads to the deflection of the Ecoflex film and its contact with the other triboelectric layer, which produces an instantaneous negative pulse voltage signal. Subsequently, the Ecoflex film restores to its original position due to its elastic response, and the sensor induces a positive pulse voltage signal. During inhalation, a small positive voltage signal is generated during inhalation, but its value is considerably smaller than that of exhalation due to the minimal suction applied to the Ecoflex film.

To demonstrate the performance of the triboelectric sensor for respiration monitoring, we conducted a synchronous measurement using our developed device and a commercial piezoelectric respiration sensor. Figure S4 in the Supporting Information shows the real-time electrical signals obtained by the two kinds of sensors, indicating that the output signals from our triboelectric sensor are comparable with that measured by the commercial sensor. Figure 3b shows the recorded signals for the four breath states: slow breath, normal breath, short breath, and deep breath. It can be seen that the new triboelectric sensor is able to distinguish the four breath states and generates unique signal patterns corresponding to the variation of respiratory rate and depth. To better identify the difference, as shown in Figure 3c, the voltage signals of respirations can be further processed by Fast Fourier transform (FFT), in which the

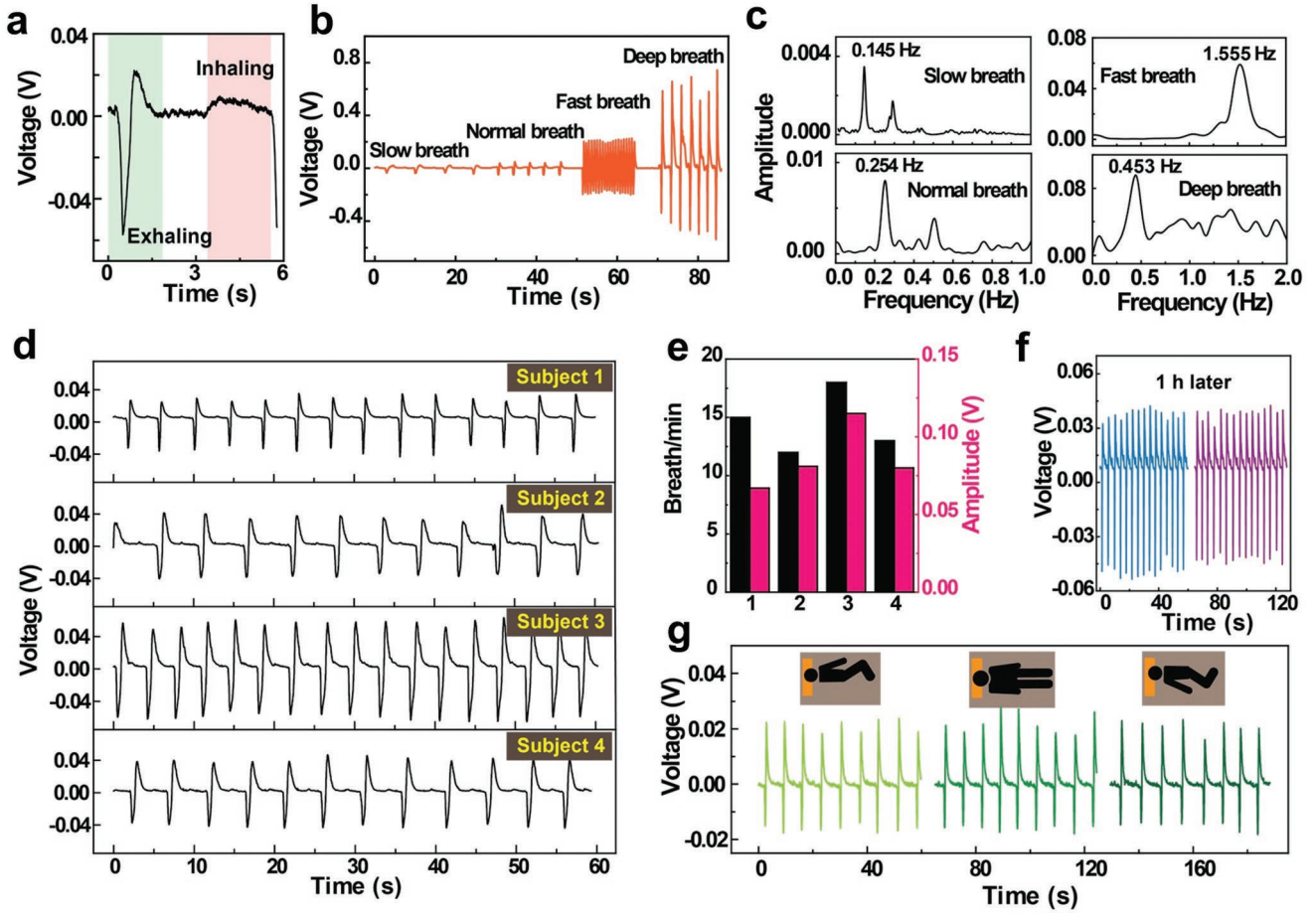

Figure 3. Real-time respiration monitoring. a) The output voltage signals for normal breath measured by the triboelectric sensor. b) The variation of the output voltage in response to different types of breath patterns: slow, normal, fast, and deep breathing. c) Fast Fourier transform (FFT) spectra of the time-dependent voltage signals shown in (b). d) The output voltage of four different volunteer subjects measured by the triboelectric sensor. e) Comparison of the respiration features of four subjects from different population groups. f) Comparison of the output voltage signals generated by the triboelectric sensor for 1 h use, indicating the good stability and reliability of the device under exhaled moisture. g) Demonstration of the real-time respiration monitoring under different lying states during sleeping. The movement of the human body has little influence on the detected output signals.

characteristic frequencies of the low breath, normal breath, fast breath, and deep breath are 0.145, 0.254, 1.555, and 0.453 Hz that are in agreement with the human respiratory rate.[34]

To verify the performance of our sensor for different individuals with diverse features, four volunteer subjects (Table S1, Supporting Information) were involved in the measurement of their normal respiration conditions. Figure 3d shows the real-time voltage signals obtained by the triboelectric sensor for four subjects, exhibiting uniform and steady respiration patterns. The four subjects have different breathing patterns (i.e., respiration rate and amplitude, Figure 3e), which can be easily distinguished by the triboelectric sensor, demonstrating its wide adaptability for different people. Actually, the size and shape of the device could be customized based on the needs and requirements of the user so that the device can be fully optimized for functionality and comfort in use.

It is noted that the exhaled breath gas contains about 40–90% relative humidity.[35] Thus, it is essential to ensure the breathing sensor to functions well under high humid conditions. However, TENGs have poor output performance and working stability in a humid environment because contact electrification is sensitive to humidity,[36,37] which may hinder the application of TENG technology in respiratory sensing. To overcome this challenge, the electrification surfaces in the triboelectric sensor in our design have no direct contact with the exhaled gas, and the edges of the device are well-sealed via silicon rubber glue (Sil-Poxy). In addition, the Ecoflex film is hydrophobic and has an excellent waterproof property to avoid water droplet condensation on the sensor. Figure 3f shows the output voltage signals of the sensor after being used for 1 h without degradation, verifying the reliability and stability for long-term use under humid conditions by exhaled water vapor.

Figure 3g shows the output voltage signals measured by the sensor when the subject is sleeping under different lying states. Our device can be fixed firmly on the nose via the magnets and the PU holder. The measured data has slight variation and noise induced by the body motions in sleeping. Thus, it will have great potential for long-time continuous respiration monitoring during sleeping. This new sensor is superior to the reported smart waist and chest belts,[38–40] which detect the variation of chest and abdomen of patience for obtaining respiration information during sleep. Their outputs and sensing performance are significantly affected by the movement of the human body.

2.4. Smart System Control by Severely Disabled People via HMI

With the advantages and robustness of the newly designed triboelectric sensor, we propose a smart breathing-driven HMI system for disabled people to control the smart system such as home appliances, smart lights, smart wheelchairs, and smart beds. The HMI system consists of a triboelectric sensor, signal processing circuits, and the target electrical appliance. In a specific application scenario (**Figure 4**a), the disabled person can actively control their respiration behavior or pattern to generate different types of signals by the triboelectric sensor. Then the generated pulse signal is amplified and processed by a microcontroller (MCU). Finally, the digital signal will be sent to the smart electrical appliance for remote operations through an ADC. The signal processing circuit used in this system consists of an amplifier & notch filter, a latching relay, and an Arduino board (Figure S5, Supporting Information). As illustrated in Figure 4b, from top to bottom, the first signal is the original signal from the triboelectric sensor with strong power-line interference, followed by the amplified and filtered signal, and the converted trigger signal to control the latching relay at the bottom. In order to accommodate the application and avoid possible impact on the normal breathing of the disabled, a threshold voltage of 3.8 V is selected, which is close to the upper limit of the signals (Figure 4b). Thus, when the disabled do deep breathing, the triboelectric sensor generates a pulse voltage larger than the defined threshold value, and a control signal will be triggered to turn on/off the electrical appliances. Figure 4c and Videos S1–S3 (Supporting Information) demonstrate the control of the different tools such as a lamp, an electric fan, and a screen by using the HMI system. In addition to the breathing-driven HMI system, we also develop an intelligent respiratory monitoring (IRM) system for detecting the health conditions of the elderly and ICU patients. As shown in Figure 4d, the IRM system can continuously monitor the breath pattern of a human. Once an abnormal breathing signal is detected, e.g., respiratory arrest, the Arduino board will send a high-level signal to trigger the alarm system or message the guardian via a smart phone. To verify the performance of this proposed IRM system, we have simulated the sleep apnea process in our lab environment. As shown in Figure 4e and Video S4 (Supporting Information), a regular respiration signal is reported without alarm warning raised when the volunteer has a typical breathing pattern. However, once the volunteer stops breathing for 10 s, the alarm will be triggered to inform the doctor or caregiver to take further action. Such an IRM system provides a new way for elderly and patient care and will be very helpful for a variety of populations to perform regular long-term real-time monitoring at home with a low-cost.

3. Conclusion

In summary, we have designed and fabricated a novel human–machine interface based on a single-electrode triboelectric sensor for respiration monitoring and smart system control in the background of building smart cities. The key parameters of the design including the distance between the nose and the device, the thickness of the Ecoflex film, and the thickness and size of the spacer have been systematically studied, and their influence on the sensing performance of the triboelectric sensor have been revealed. We further demonstrated its potential applications as a self-powered respiration sensor for detecting various breath states for a variety of populations. Based on the triboelectric sensor, we developed a smart breath-driven HMI system that can convert real-time respiration signals into control signals for electrical appliances. Finally, an intelligent respiratory monitoring system was built to monitor the respiratory arrest of patients and the elderly. This research provides a promising strategy for real-time respiratory monitoring of the elderly and patient care and promises to make new advances on self-powered HMIs for severely disabled people in a home environment.

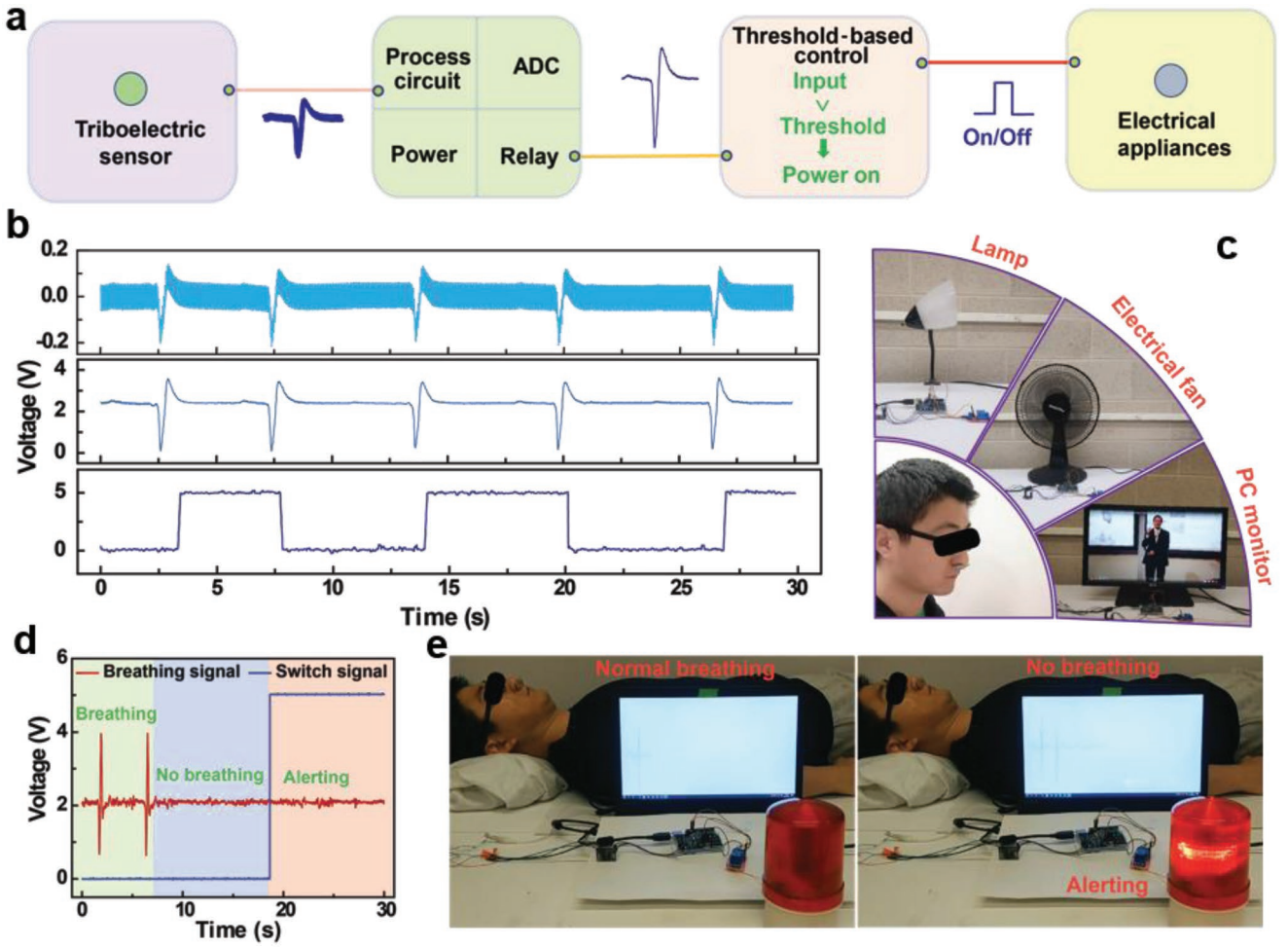

Figure 4. Demonstration of the HMI system for the disabled. a) Schematic diagram of the designed TENG-based HMI system. b) From top to bottom, the first signal is the original breathing signal from the TENG. The second one shows the voltage signal after being filtered and amplified. The final one shows the converted trigger signal. c) Demonstration of the control of household appliances via the HMI system. d) The breathing and switch signals when the volunteer breaths normally or stops breathing. e) Demonstration of the intelligent respiratory monitoring (IRM) system for respiratory arrest alarm. When the patient stops to breathing for 10 s, the alarm will be triggered to inform the doctors or caregivers.

4. Experimental Section

Fabrication of the triboelectric sensor: A circular-shaped PET substrate with eight holes along its edge was fabricated by using a laser cutter (Glowforge plus). The circular spacers with different thicknesses and diameters were printed with PLA by a Zmorph-2.0-SX 3D printer. To obtain the super-thin Ecoflex film, liquid parts A and B of the Ecoflex-30 silicon rubber were mixed with a volume ratio of 1:1. The Ecoflex mixture was spin-coated on a sandpaper template (P1000) and then cured at 80 °C for 20 min. The Ecoflex film was then peeled off from the template. Finally, the as-prepared several components were assembled to form the triboelectric sensor.

Characterization and Measurement of the Device: The experimental setup is presented in Figure S1 in the Supporting Information. The pressure meter was used to tune the applied air pressure. The linear motor (LinMot MBT-37 120) was employed to switch on and off the airflow for accurate frequency control. Two circular air vents with a diameter of 10 mm were located above the sensor. The sensor was designed based on the single-electrode mode, connecting with a 500 MΩ resistor. A current preamplifier (Keithley 6514 System Electrometer) was used to measure the voltage signals of the resistor. The software LabVIEW was programmed to acquire real-time control and data extraction. The photographs of the Ecoflex film were characterized by using an optical microscope (Olympus SZX12). Evaluation and demonstration experiments involved with human subjects (i.e., volunteers) were approved by appropriate ethics committee and written consent of all participants were obtained.

Numerical Modeling of the Sensing Mechanism and Structure Optimization: The potential distribution of the triboelectric sensor was simulated by the software package COMSOL 5.4. The triboelectric charge density on the inner surface was assigned as 1 μC m^{-2}. The deformation of the Ecoflex layer was further modeled by finite element method (FEM) with the software package ABAQUS 6.14. The 4-node tetrahedral element was used to discretize the thin membrane. The Ogden constitutive model was utilized to fit the property of Ecoflex 00–30 with the parameters: $\mu_1 = 0.001887$; $\alpha_1 = -3.848$; $\mu_2 = 0.02225$; $\alpha_2 = 0.663$; $\mu_3 = 0.003574$; $\alpha_3 = 4.225$; $D_1 = 2.93$; $D_2 = 0$; $D_3 = 0$. Uniform air pressure was applied vertically to the free-moving surface of the membrane, and 3 translational degrees of freedom of the outer bottom surface of the silicone layer are fixed (Ecoflex layer attached to the spacer).

Supporting Information

Supporting Information is available from the Wiley Online Library or from the author.

Acknowledgements

This work was partially supported by National Science Foundation (ECCS-2024649), US DOT (693JK32050003CAAP), and Case Western Reserve University.

Conflict of Interest

The authors declare no conflict of interest.

Data Availability Statement

The data that support the findings of this study are available from the corresponding author upon reasonable request.

Keywords

human–machine interface, respiratory monitoring, self-powered sensors, smart system control, triboelectric nanogenerators

Received: May 31, 2022
Revised: June 1, 2022
Published online:

[1] X. Qu, Y. Liu, Z. Liu, Z. Li, *J. Phys.: Mater.* **2021**, *4*, 034015.
[2] Disability and health, www.who.int/news-room/fact-sheets/detail/disability-and-health (accessed: November 2021).
[3] S. Sundaram, P. Kellnhofer, Y. Li, J. -. Y. Zhu, A. Torralba, W. Matusik, *Nature* **2019**, *569*, 698.
[4] V. Ravindra, C. Castellini, *Front. Neurorobot.* **2014**, *8*, 1.
[5] K. Kim, J. Kim, J. Choi, J. Kim, S. Lee, *Sensors* **2015**, *15*, 1022.
[6] K. Dong, Z. Wu, J. Deng, A. C. Wang, H. Zou, C. Chen, D. Hu, B. Gu, B. Sun, Z. L. Wang, *Adv. Mater.* **2018**, *30*, 1804944.
[7] M. Amjadi, K.i-U.k Kyung, I. Park, M. Sitti, *Adv. Funct. Mater.* **2016**, *26*, 1678.
[8] O. Bazanova, *J. Behav. Brain Sci.* **2012**, *2*, 4.
[9] Y. Zhao, S. Yao, S. Hu, S. Chang, R. Ganti, M. Srivatsa, S. Li, T. Abdelzaher, *IEEE International Conference on Big Data (Big Data)*, Boston, MA **2017**, p. 1709.
[10] O. Aydemir, T. Kayikcioglu, *J. Neurosci. Methods* **2014**, *229*, 68.
[11] M. Simao, N. Mendes, O. Gibaru, P. Neto, *IEEE Access* **2019**, *7*, 39564.
[12] M. Pang, S. Guo, Q. Huang, H. Ishihara, H. Hirata, *J. Med. Biol. Eng.* **2015**, *35*, 165.
[13] O. Asan, Y. Yang, *JMIR Hum. Factors* **2015**, *2*, e5.
[14] P. Biswas, P. Langdon, *J. Assist. Technol.* **2011**, *5*, 58.
[15] F. L. Coutinho, C. H. Morimoto, *Int. J. Comput. Vis.* **2013**, *101*, 459.
[16] K. Holmqvist, P. Blignaut, *Behav. Res. Methods* **2020**, *52*, 2098.
[17] B. N. Johnson, J. D. Mainland, N. Sobel, *J. Neurophysiol.* **2003**, *90*, 1084.
[18] A. Plotkin, L. Sela, A. Weissbrod, R. Kahana, L. Haviv, Y. Yeshurun, N. Soroker, N. Sobel, *Proc. Natl. Acad. Sci. USA* **2010**, *107*, 14413.
[19] Z. L. Wang, *Adv. Energy Mater.* **2020**, *10*, 2000137.
[20] J. Luo, W. Gao, Z. L. Wang, *Adv. Mater.* **2021**, *33*, 2004178.
[21] Y. Pang, Y. Cao, M. Derakhshani, Y. Fang, Z. L. Wang, C. Cao, *Matter* **2021**, *4*, 116.
[22] W. Li, G. Liu, D. Jiang, C. Wang, W. Li, T. Guo, J. Zhao, F. Xi, W. Liu, C. Zhang, *Adv. Mater. Technol.* **2018**, *3*, 1800189.
[23] Z. Ren, L. Wu, J. Zhang, Y. Wang, Y. Wang, Q. Li, F. Wang, X.i Liang, R. Yang, *ACS Appl. Mater. Interfaces* **2022**, *14*, 5497.
[24] Y. Pang, S. Chen, Y. Chu, Z. L. Wang, C. Cao, *Nano Energy* **2019**, *66*, 104131.
[25] X. Pu, H. Guo, J. Chen, X. Wang, Y.i Xi, C. Hu, Z. L. Wang, *Sci. Adv.* **2017**, *3*, e1700694.
[26] H. Zhou, D. Li, X. He, X. Hui, H. Guo, C. Hu, X. Mu, Z. L. Wang, *Adv. Sci.* **2021**, *8*, 2101020.
[27] S. Chen, Y. Pang, H. Yuan, X. Tan, C. Cao, *Adv. Mater. Technol.* **2020**, *5*, 1901075.
[28] Y. Pang, J. Li, T. Zhou, Z. Yang, J. Luo, L. Zhang, G. Dong, C. Zhang, Z. L. Wang, *Nano Energy* **2017**, *31*, 533.
[29] B. Zhang, Y. Tang, R. Dai, H. Wang, X. Sun, C. Qin, Z. Pan, E. Liang, Y. Mao, *Nano Energy* **2019**, *64*, 103953.
[30] M. Wang, J. Zhang, Y. Tang, J. Li, B. Zhang, E. Liang, Y. Mao, X. Wang, *ACS Nano* **2018**, *12*, 6156.
[31] P. Cheng, H. Guo, Z. Wen, C. Zhang, X. Yin, X. Li, D.i Liu, W. Song, X. Sun, J. Wang, Z. L. Wang, *Nano Energy* **2019**, *57*, 432.
[32] S. Niu, S. Wang, L. Lin, Y. Liu, Y. Zhou, Y. Hu, Z. L. Wang, *Energy Environ. Sci.* **2013**, *6*, 3576.
[33] J. Zhong, Q. Zhong, F. Fan, Y. Zhang, S. Wang, B. Hu, Z. L. Wang, J. Zhou, *Nano Energy* **2013**, *2*, 491.
[34] Z. Zhang, J. Zhang, H.e Zhang, H. Wang, Z. Hu, W. Xuan, S. Dong, J. Luo, *Nanoscale Res. Lett.* **2019**, *14*, 354.
[35] E. Mansour, R. Vishinkin, S. Rihet, W. Saliba, F. Fish, P. Sarfati, H. Haick, *Sens. Actuators, B* **2020**, *304*, 127371.
[36] L. Li, X. Wang, P. Zhu, H. Li, F. Wang, J. Wu, *Nano Energy* **2020**, *70*, 104476.
[37] R. Wen, J. Guo, A. Yu, J. Zhai, Z. L. Wang, *Adv. Funct. Mater.* **2019**, *29*, 1807655.
[38] H.e Zhang, J. Zhang, Z. Hu, L. Quan, L. Shi, J. Chen, W. Xuan, Z. Zhang, S. Dong, J. Luo, *Nano Energy* **2019**, *59*, 75.
[39] S. Park, P. Das, A. Chhetry, J. Park, *IEEE Sens. J.* **2017**, *17*, 6558.
[40] F. Yi, L. Lin, S. Niu, P.o K. Yang, Z. Wang, J. Chen, Y. Zhou, Y. Zi, J. Wang, Q. Liao, Y. Zhang, Z. L. Wang, *Adv. Funct. Mater.* **2015**, *25*, 3688.